

A FRAMEWORK FOR UNDERSTANDING THE TOPOLOGY OF COMPLEX CORONAL STRUCTURES

D. I. PONTIN¹, E. R. PRIEST¹ and D. W. LONGCOPE²

¹*School of Mathematics and Statistics, University of St. Andrews, St. Andrews,
Fife, KY16 9SS, Scotland, U.K.*

²*Department of Physics, Montana State University, Bozeman, MT 59717, U.S.A.*

(Received 21 June 2002; accepted 1 October 2002)

Abstract. The Sun's coronal magnetic field is highly complex and provides the driving force for many dynamical processes. The topology of this complex field is made up mainly of discrete topological *building blocks* produced by small numbers of magnetic fragments. In this work we develop a method for predicting the possible topologies due to a potential field produced by three photospheric sources, and describe how this model accurately predicts the results of Brown and Priest (1999). We then sketch how this idea may be extended to more general non-symmetric configurations. It is found that, for the case of positive total flux, a local separator bifurcation may take place with three positive sources or with one positive and two negative sources, but *not* for two positive sources and one negative.

1. Introduction

The topology of a magnetic field includes the connectivity of its field lines, which for the solar corona is very complex (Berger, 1986; Longcope, 1996, 1998). Such connectivity is encapsulated elegantly within the so-called *topological skeleton* of the field (Priest, Bungey, and Titov, 1997). A topological skeleton includes the set of photospheric flux sources that produce the magnetic field together with the null points and their spines, fans and separators.

We consider here a potential coronal magnetic field, with the flux sources being situated in the photosphere (Schrijver and Zwaan, 2000; Title, 2000; Hagenaar, 2001), which is treated locally as a plane (chosen to be $z = 0$). Since the field is potential, our flux sources are represented as point sources, whose strength (ε) is given by the magnetic flux through any dome within which the source lies, divided by 2π . Then the total magnetic field at a point \mathbf{r} due to sources of strength ε_i at position \mathbf{r}_i is given by

$$\mathbf{B}(\mathbf{r}) = \sum_i \frac{\varepsilon_i (\mathbf{r} - \mathbf{r}_i)}{|\mathbf{r} - \mathbf{r}_i|^3}. \quad (1)$$

Although magnetic monopoles do not of course exist in the interior of a volume, we are allowed to place them on a boundary (the photosphere) in order to model



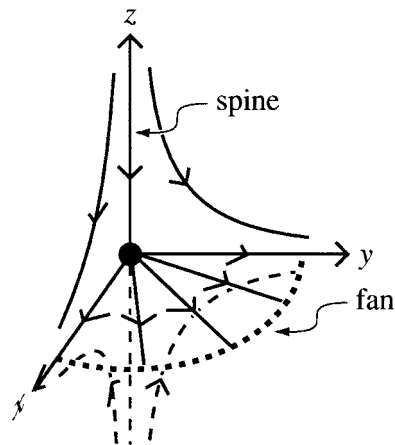


Figure 1. The local field structure of a first-order proper radial null point.

the locations where magnetic flux passes through the photosphere from below the solar surface into the corona.

Other than flux sources (Démoulin, Hénoux, and Mandrini, 1992, 1994; Parnell, 2001; Simon, Weiss, and Title, 2001), the main components of a topological skeleton are the null points of the field and their associated spine field lines and fan planes (Priest and Forbes, 2000). A *null point* is a location at which the magnetic field vanishes ($\mathbf{B} = 0$). The field in the vicinity of a null can be described by three eigenvalues, which are all real in a potential field, and which sum to zero since $\nabla \cdot \mathbf{B} = 0$. One eigenvalue must hence be of opposite sign to the other two, and its associated eigenvector gives an isolated field line passing through the null known as the *spine* field line (Priest and Titov, 1996). The other two eigenvectors form a plane (locally perpendicular to the spine in a potential field) in which field lines radiate out from (or in towards) the null, called the *fan* surface (see Figure 1). The fan field lines make up fan surfaces which can spread into space as separatrix surfaces that separate regions of different field line connectivity.

One further component which may or may not be present in the skeleton of a field is a *separator* which is a special field line connecting two null points directly and representing the intersection of two fans.

Null points can be classified according to their position and orientation. If all flux sources lie in a plane, a null which is present above the source plane (the photosphere) is known as a *coronal* null. Nulls which occur in the photosphere can be split into two groups depending on whether their spines locally lie perpendicular or parallel to the photospheric plane (these are the only two possibilities for nulls in the photosphere if the field is potential and all the sources lie in the photosphere). Nulls whose spines are perpendicular to the photosphere are said to be *upright*, whereas those whose spines lie parallel to it are said to be *prone*. We can further classify these nulls by giving them signs. They are termed positive or negative

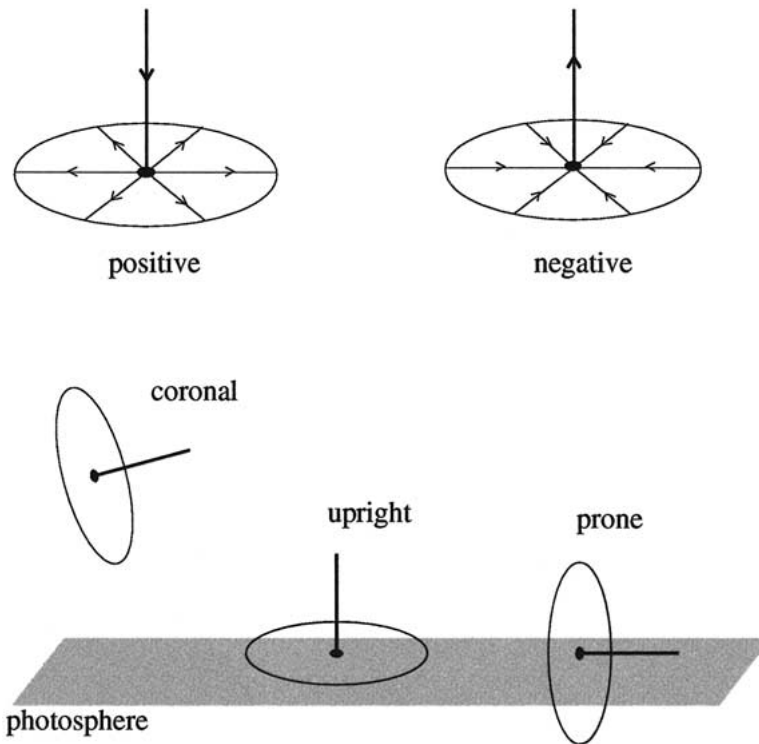


Figure 2. The spines (*thick lines*) and fans (*discs*) for the different types of null point which may be present in a potential coronal magnetic field.

according to whether the field lines in the fan point away from the null or towards it, respectively (Figure 2).

In the analysis which follows, we shall first consider the topologies due to three photospheric sources, which have all been classified by Brown and Priest (1999). The eight distinct topologies are shown in Figure 5. The question is: can we understand why these topologies occur, in particular why some sets of sources allow local bifurcations from their basic states to more complex ones (touching, triangular) whereas others do not? If we can understand this, then we will be well-equipped to predict allowed topologies for larger numbers of sources, where manually searching parameter-space is impossibly time-consuming. In this way we can develop a tool for modeling real coronal fields.

We start by giving a brief description of Euler characteristics and an overview of the behavior of the nulls which take part in a particular type of local bifurcation. We then go on to describe three-source topology, which leads to the question of how we might go about understanding why the observed topological states occur. In Section 2.4 we propose an analytical model for the local separator bifurcation. Section 3 compares the bifurcation model with the three-source states which are

observed to bifurcate in this way, and puts forward an explanation as to why the other states may not do so.

2. Bifurcations

2.1. EULER CHARACTERISTICS

The numbers of sources/sinks and nulls in a potential vector field are related by Euler characteristics (or Poincaré indices) (Seehafer, 1986; Gorbachev, 1988; Dubrovin, Fomenko, and Novikov, 1990). In the limit of infinite contour/surface radius in the calculation of these characteristics (which is appropriate for an isolated system), they become, in 2D (Inverarity and Priest, 1999):

$$S_+ + n_{u+} + S_- + n_{u-} = n_{p+} + n_{p-} + \begin{cases} 1 & q \neq 0 \\ 2 & q = 0 \end{cases} \quad (2)$$

and in 3D:

$$S_+ - S_- = n_{u+} + n_{p+} + n_{c+} - n_{u-} - n_{p-} - n_{c-} + \begin{cases} \text{sign}(q) & q \neq 0 \\ 0 & q = 0, \end{cases} \quad (3)$$

where

$$\left\{ \begin{array}{ll} S_{+/-} & \text{is the number of positive/negative sources,} \\ n_{p+/-} & \text{is the number of positive/negative prone nulls,} \\ n_{u+/-} & \text{is the number of positive/negative upright nulls,} \\ n_{c+/-} & \text{is the number of positive/negative coronal nulls,} \\ q & \text{is the sum of the source and sink fluxes.} \end{array} \right.$$

The 2D characteristic is calculated for the photosphere, and the 3D characteristic for all space. In this paper we verify that the constraints inferred from these characteristics are indeed satisfied, when new states arise due to the addition of new sources or the bifurcation of nulls. More generally, when dealing with a large number of sources (e.g., Inverarity and Priest, 1999), the characteristics provide a useful check on whether or not all the null points have been detected.

2.2. LOCAL SEPARATOR BIFURCATION

A *local bifurcation* is a bifurcation in which nulls are created or destroyed, and thus the local field-line connectivity is changed (Hornig and Schindler, 1996). A *local separator bifurcation* (Brown and Priest, 1999) (see Figure 3) is a saddle-node bifurcation in which either a second-order null is created and splits into two

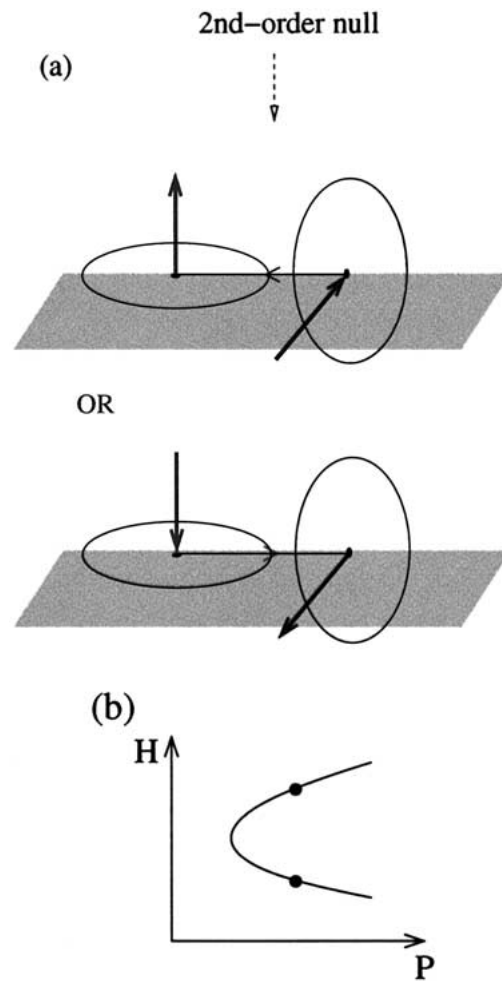


Figure 3. (a) The structure of the nulls created in a local separator bifurcation. (b) Schematic representation of a saddle-node bifurcation, where H is the horizontal position of the null and P is a control parameter.

new first-order nulls, or the reverse occurs and two first-order nulls coalesce to form a second-order null which is subsequently annihilated. All of this happens in the photosphere for our set of potential sources placed in the photosphere. Of the two first-order nulls, one is positive and one is negative, while one is upright and one is prone (see Figure 3(a)). The skeletal structure of the field around such a pair of null points is shown in Figure 4. Note that this bifurcation always ensures that the system continues to satisfy the Euler characteristics, since increasing n_{u+} and n_{p-} , say, by 1 does not produce a net change in the terms in both Equations (2) and (3).

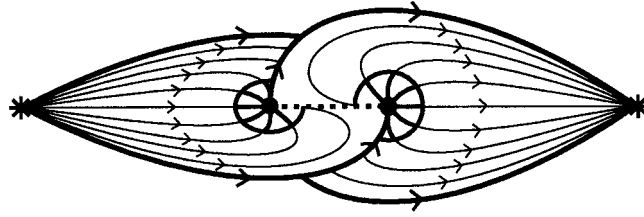


Figure 4. The skeletal field structure near a pair of null points (*large dots*) created in a local separator bifurcation. The *discs* represent the fans of the two nulls and the *thick lines* the spines. The *dotted line* is a separator and the *stars* are sources.

2.3. TREE DIAGRAM FOR THREE SOURCES

The analysis which follows involves performing a thought experiment where we start with a known (allowed) configuration of sources and nulls and consider the effect of adding further sources. If the new source is very weak compared to the existing source(s), then close to the new source there appears also a prone positive (or negative) null if the source is positive (or negative, respectively). The source strength can then be increased, and local bifurcations to new states may eventually occur. Note that we will always continue to satisfy the Euler characteristics in this way, since adding a small source increases both S_+ and n_{p+} , say, by 1. Indeed, neither adding a small source nor allowing a local bifurcation has a net effect on Equations (2) and (3). New states may also be created by global bifurcations, in which there is a global change of connectivity, but the number and nature of the nulls are unchanged, and they are outside the scope of our treatment here. Furthermore, as we consider only sources in the plane and the local separator bifurcation, we will here concentrate on nulls that lie in the photospheric plane.

The different sets of sources and nulls that we arrive at are shown in Figure 6. Consider starting with a single positive (say) source on the extreme left of the Figure. Adding another positive source to this simply gives two positive sources and one positive prone null (p_+). This remains the case regardless of the source positions and strengths. Let us call this the *two-source wall* state. Adding a weak negative source (S_-), on the other hand, produces a negative prone null (p_-), so we have one source of each sign with a negative prone null. This state will remain in existence as long as the negative source is weaker than the positive source. In the topological skeleton of this state the weaker source is enclosed within the fan of the null point, so call it a *dome* state with positive total flux. However, if the weaker source becomes stronger, a global bifurcation will occur to a new dome state with a positive prone null instead of a negative one and a negative total flux.

For clarity and without loss of generality, we consider here only states with positive total flux. All of the topologies described also occur with negative total flux and reversed polarity. These negative flux states can be reached by global bifurcations from the two- or three-source states with positive total flux, by increasing the strengths of their negative sources.

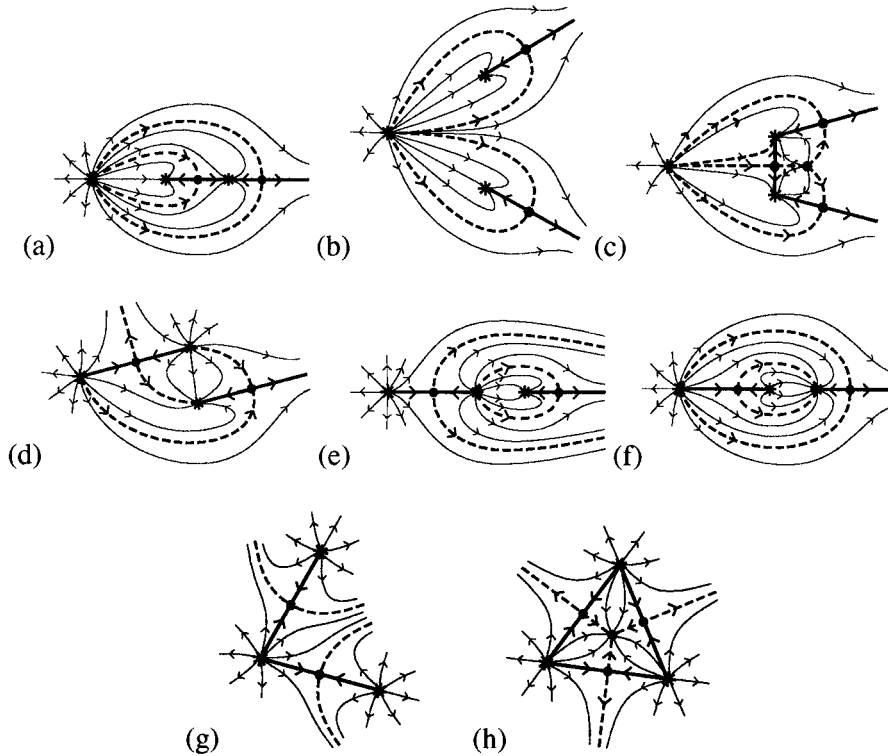


Figure 5. The intersections with the photosphere made by the eight topologies due to three photospheric sources (Brown and Priest, 1999). (a) Enclosed, (b) separate, (c) touching, (d) intersecting, (e) detached, (f) nested, (g) divided, and (h) triangular states. Here the sources are shown as *stars*, the nulls by *large dots*, the spines by *thick curves*, the separatrix fans by *dashed curves*, and additional field lines in each domain by *thin curves*.

Consider now the effect of adding more weak positive or negative sources to the wall and dome states with positive total flux. From the wall state if we add a further positive source then we will obtain the *three-source divided* state. As the strengths and positions of the three sources are changed, a local separator bifurcation may occur to the *triangular* state, in which, in addition to the original two positive prone nulls there is an extra positive prone null (p_+) and an upright negative null (u_-). The reasons for the presence of such a bifurcation will be discussed in Section 3.

Consider next the addition of a negative source to the wall state with positive total flux. As discussed above, this will give birth to a negative prone null, in addition to the positive one which is already present. We can obtain the same state by instead adding a positive source to the two-source dome state with positive total flux. In this case we gain a positive prone null and again end up with two positive sources, one negative source, and positive total flux, and therefore one positive and one negative prone null. Depending on the source positions and strengths, the topology may be either *detached*, *intersecting* or *nested*, with global bifurcations

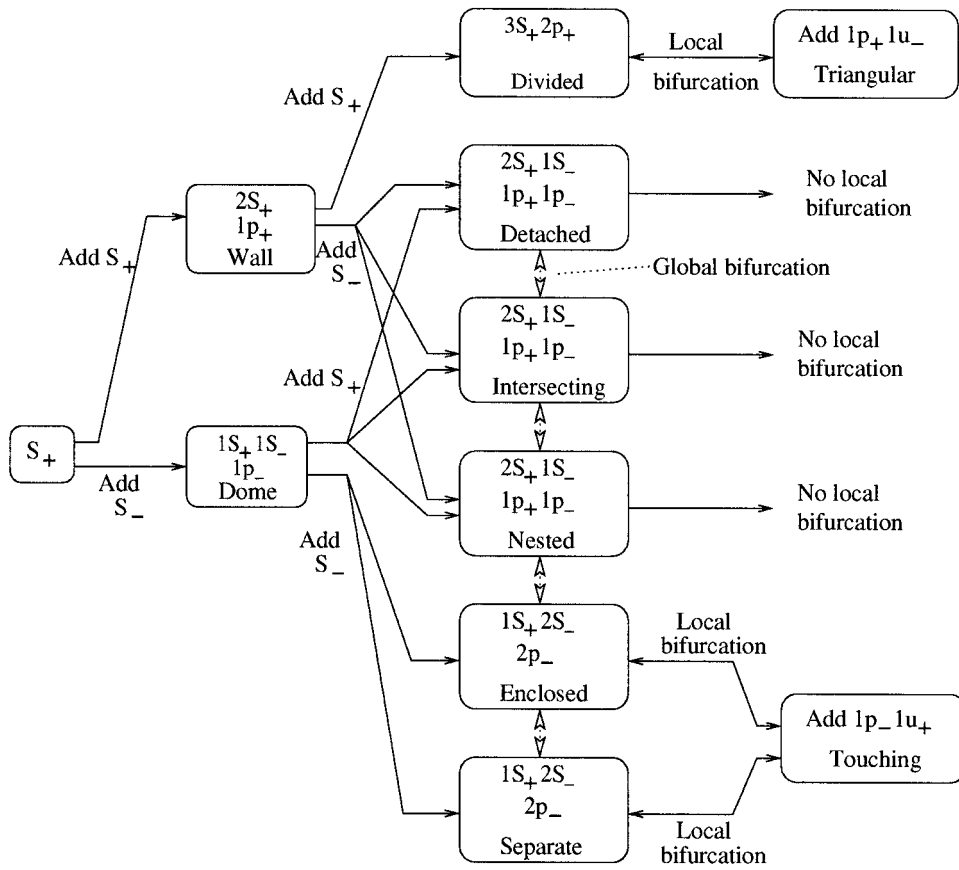


Figure 6. Diagram showing how the different three-source topologies with positive total flux can be built up by starting with one positive source (S_+) and adding further weak sources of positive (S_+) or negative (S_-) polarity. The presence of prone positive (p_+) and negative (p_-) nulls is indicated, together with the effects of global and local bifurcations, which sometimes involve the creation of upright nulls (u_+ or u_-).

possible between these topological states. No local bifurcations occur from them, for reasons discussed in Section 3. When the total flux is close to zero, the state has the nested topology. From this state, if the strength of the negative source is increased so as to make the total flux negative, a global bifurcation takes place into the enclosed state.

Finally, suppose we add a negative source to the dome state with positive total flux. In doing so, we arrive at either the enclosed state or the separate state, and again global bifurcations between these states may occur. For the right source configuration, we may have a local bifurcation from either of these states into the *touching* state, in which an extra positive prone null and an extra upright negative null are present. A state which has the touching topology may locally bifurcate into either the enclosed or the separate state.

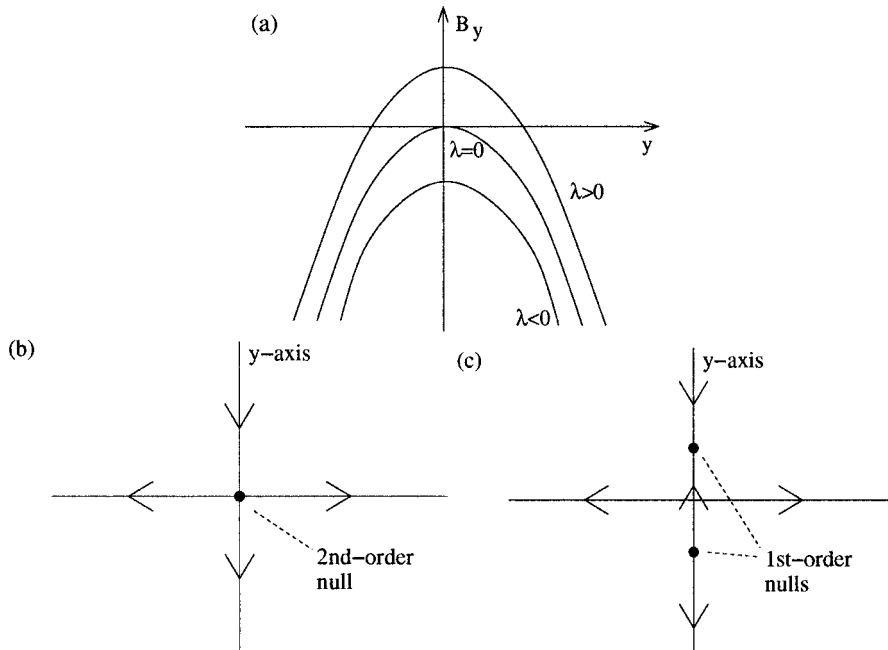


Figure 7. (a) The variation with y of the magnetic field component B_y along the y -axis for the field $\mathbf{B} = (x(1 + 2y), \lambda + x^2 - y^2, -z)$ when λ is positive, zero, and negative. (b) and (c) show schematic diagrams of the field structure during a local separator bifurcation when (b) a second-order null splits into (c) two first-order nulls or *vice versa*.

2.4. SIMPLE ANALYTICAL MODEL FOR LOCAL SEPARATOR BIFURCATION

The crucial field structure required for a local separator bifurcation is a second-order null point. Consider the field

$$\mathbf{B} = (x(1 + 2y), \lambda + x^2 - y^2, -z), \tag{4}$$

where λ is a constant, which is the simplest example of a potential field which exhibits second-order behavior (while still satisfying $\nabla \cdot \mathbf{B} = 0$ and $\nabla \times \mathbf{B} = 0$).

When $\lambda < 0$, no nulls are present. When $\lambda = 0$, a second-order null appears at the origin. When $\lambda > 0$ there are two first-order nulls at $(0, \sqrt{\lambda}, 0)$ and $(0, -\sqrt{\lambda}, 0)$ (see Figure 7(a)). As we can see from (4), the structure of the field near a second-order null is as follows. In one plane (here the xz -plane) it has the hyperbolic topology of an X-type null point. In a direction perpendicular to this plane the field is everywhere in one direction, but falls in magnitude to zero at one point. If we perturb such a field by adding a small positive λ , the second-order null will split into two first-order nulls. Note that to each side of this newly-created pair of first-order nulls the field (B_y) retains its original direction, while this direction is reversed between them. The skeletal structure of the field between such a pair of null points is shown in Figure 4.

In the xz -plane, close to the y -axis, the field behaves like a typical 2D hyperbolic null, so that the field is directed everywhere away from the y -axis in the photosphere (or towards it if $(1 + 2y)$ is replaced by $(-1 + 2y)$ in the x -component of \mathbf{B} in Equation (4) whereupon the z -component must become $+z$). From the above analysis, we might expect the local behavior near a second-order null point during bifurcation to have the structure shown in Figures 7(b) and (c).

Note that the magnetic field (4) also possesses zeros at $(\sqrt{\frac{1}{4} - \lambda}, -\frac{1}{2}, 0)$ and $(-\sqrt{\frac{1}{4} - \lambda}, -\frac{1}{2}, 0)$, when $\lambda < \frac{1}{4}$. As λ increases towards $\frac{1}{4}$ the nulls approach along the line $y = -\frac{1}{2}, z = 0$. They coalesce at $\lambda = \frac{1}{4}$ and no longer exist when $\lambda > \frac{1}{4}$.

3. Three Sources

Now let us try to understand why a divided, enclosed or separate state can undergo a local bifurcation through the creation of a second-order null, whereas a detached, intersecting or nested state cannot.

3.1. GENERAL CONSIDERATIONS

Consider two positive (say) sources in a region of the photosphere with no ambient field. Between such sources a null is present, whose spine connects them and whose fan is a separatrix wall. The intersection of the fan with the photosphere is a straight line if the two sources are of equal strength, but in general for unequal sources the wall curves around the weaker source. In the photosphere, the magnetic field lies along the direction of the separatrix curve since it is a field line. Across the curve there is an opposition of the field from the two sources, and in a plane perpendicular to it the field looks like the hyperbolic null structure described in the previous section. Now consider adding a third (photospheric) source to this configuration.

For a configuration of three sources, there are three distinct situations which exhibit quite separate behavior with respect to the topologies that they form and the bifurcations between these topologies. Firstly, there is the case of three positive (say) sources. Secondly, we may have two positive sources and one negative source with the total flux being negative and, thirdly, the same set of sources but with a total positive flux. (These situations are equivalent to those with reversed polarity, i.e., three negative sources or two negative sources and one positive source, which do not therefore need to be considered separately.)

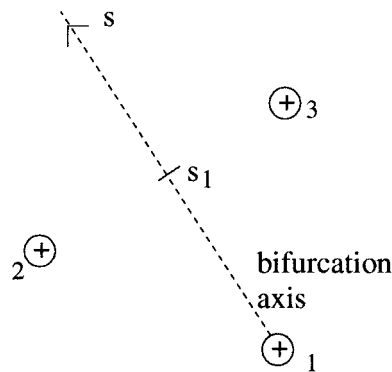


Figure 8. Diagram showing the parameterization used for constructing the bifurcation axis argument. The dashed line is the bifurcation axis, along which s increases, from $s = 0$ at source 1. s_1 is the point midway between sources 2 and 3.

3.2. THREE SYMMETRIC SOURCES

3.2.1. Three Positive Sources

If the added source (source 1 in Figure 8) is of a suitable strength, then the two nulls that are formed join this new source, via their spines, to the other two sources (2 and 3). (If not, the configuration will be an equivalent rotation of this, so long as the sources are placed in a roughly triangular shape.) The separatrix fans of these nulls run up between the two original sources as shown in Figure 5(g).

The simplest case is the symmetric case when F_2 (the strength of source 2) is equal to F_3 (the strength of source 3), and source 1 is placed on the perpendicular bisector of the line between sources 2 and 3, which we refer to as the *bifurcation axis*. The field (B_1) due to source 1 is parallel to the bifurcation axis, and, due to the symmetry of the situation, the components perpendicular to this axis of the fields of sources 2 and 3 cancel one another. If we take a cross-section through the bifurcation axis, the field in this plane has a hyperbolic null structure. It is likely, therefore, that this axis may be a good candidate to act as the y -axis in the analysis of Section 2.4.

Along the bifurcation axis B_1 decays in the usual inverse-square law fashion. Consider the parameterization shown in Figure 8, where s is the distance along the bifurcation axis from source 1 and s_1 marks the point midway between sources 2 and 3. For small s ($s/s_1 \ll 1$), the field (B_s) along the bifurcation axis is in the direction of increasing s , i.e., $B_s > 0$ since B_1 dominates. For $s > s_1$, $B_s > 0$ always, since B_1 , B_2 and B_3 are all in the positive s -direction. However, for $s < s_1$ the field (B_{2+3}) along the bifurcation axis due to sources 2 and 3 combined opposes B_1 . If B_1 and B_{2+3} are equal and opposite at some point, then there will be a null there. The variation of B_{2+3} with s is shown schematically in Figure 9.

Three possible composite profiles for B_s are shown in Figure 9. As the strength of source 1 is decreased, the B_1 curve drops until it touches (dashed line) and then

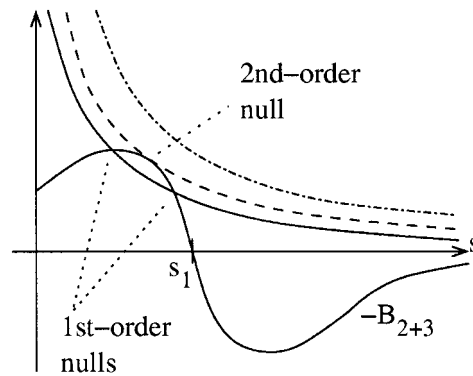


Figure 9. The field profiles along the bifurcation axis for three positive sources due to source 1 (B_1) and sources 2 and 3 (B_{2+3}). B_1 profiles are shown *dot-dashed* before bifurcation, *dashed* at the point of appearance of the second-order null, and *solid* after bifurcation.

cuts (solid line) the curve $-B_{2+3}$, thus creating two first-order nulls. The transition between the dot-dashed and solid B_1 curves in Figure 9 is analogous to increasing λ from $\lambda_1 < 0$ to $\lambda_2 > 0$. They correspond, respectively, to the divided and triangular topological states shown in Figures 5(g) and 5(h).

3.2.2. Two Positive Sources and One Negative

Now consider the case of two positive sources and one negative source, keeping to a symmetric configuration for simplicity. We want to look for the possibility of having a second-order null, so consider the case where the positive sources have equal strength and the negative source lies on their perpendicular bisector. Call this line, once again, the bifurcation axis (we replace the positive source 1 in Figure 8 with a negative source). A hyperbolic null structure will be present between the two positive sources, as before, in a plane perpendicular to the bifurcation axis.

(A) Negative Total Flux

In the case of negative total flux, since the negative source (1) is stronger than the sum of the two positive sources for $s/s_1 \gg 1$, far away from source 1 B_s is negative. B_s is also negative for $s < s_1$, since B_1 and B_{2+3} are both negative there. For $s > s_1$, B_1 and B_{2+3} oppose one another and so may cancel. $B_{2+3}(s)$ will again have the type of profile shown in Figure 9.

Can we obtain a second-order null on the bifurcation axis in this case? Consider Figure 10(a). From this graph we can see that it is indeed possible. Note that for the dashed and dot-dashed B_1 curves, when the curve for B_{2+3} moves down and touches the curve for B_1 , it climbs up above it again because B_1 dominates B_{2+3} at large distances. So, if the positive sources can be moved in such a way that at some point, or in some region, $|B_{2+3}| > |B_1|$ then a local bifurcation will occur. From Figure 10(a), we expect the second-order null to appear at some point $s' > s_1$. Note that, as in the case of three positive sources, the second-order null is created at the

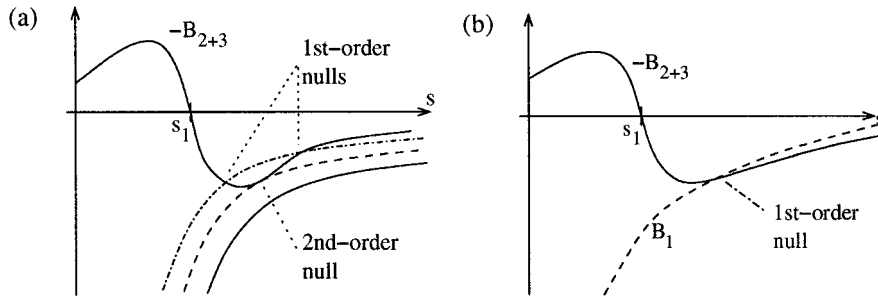


Figure 10. (a) The field profiles along the bifurcation axis for one negative and two positive sources with negative total flux. B_1 is shown *solid* before bifurcation, *dashed* at the point of appearance of the second-order null, and *dot-dashed* after bifurcation. The case when the total flux is positive is shown in (b).

point where a separatrix line splits, or equivalently, where two separatrices initially become coincident (see Figure 5(c)). Note also that the second-order null appears at $s' > s_1$, as predicted in the bifurcation axis analysis. Once again, the curves in Figure 10(a) can be considered as analogous to $\lambda < 0$, $\lambda = 0$ and $\lambda > 0$. In a general non-symmetric configuration (Section 3.3), the case of negative total flux corresponds to the enclosed and separate states, with the touching state being the bifurcated state (see Figures 5(a–c)). In the non-generic symmetric configuration described above we have the separate and touching states, and a special form of the enclosed state, shown in Figures 12 and 13 in Priest, Bungey, and Titov (1997).

(B) Positive Total Flux

In the case of positive total flux, B_s is positive for $s/s_1 \gg 1$, since the negative source is weaker than the sum of the two positive sources. For $s/s_1 \ll 1$, however, $B_s < 0$. So there must always be a first-order null on the bifurcation axis where B_s changes direction. For $s < s_1$, B_1 and B_{2+3} are both negative, so the null must be at some distance $s' > s_1$. In this case it is not possible to create a second-order null (a null on both sides of which the field is in the same direction) as shown in Figure 10(b). This is because B_1 decays more quickly than B_{2+3} at large distances so that, once $|B_1|$ drops to $|B_{2+3}|$, it will fall further and further below it. This explains why there are no local bifurcations in the case of two positive sources and one negative source with positive total flux. This case corresponds to the topologies shown in Figure 5(d–f), which show the intersecting, detached and nested states.

3.3. THREE-SOURCE NON-SYMMETRIC STATES

We now extend the symmetric case described in the previous section to consider a general non-symmetric configuration, where source 1 does not lie on the perpendicular bisector of 2–3 and $F_2 \neq F_3$. We parametrise this non-symmetric problem as follows, by working in plane polar coordinates with respect to source 1 situated at the origin. Sources 2 and 3 are placed at (r_2, ϕ_2) and (r_3, ϕ_3) , respectively, and

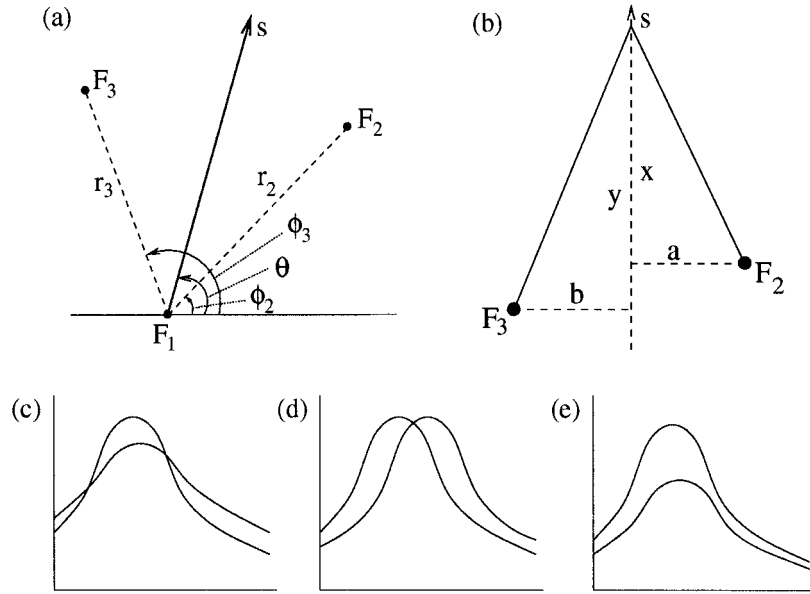


Figure 11. (a) The general parameterization for a three-source non-symmetric state and (b) the parameterization used to consider the field at large distances. (c–e) show schematic field profiles for B_2 and $-B_3$ for the cases when B_\perp has (c) two zeros, (d) one zero, and (e) no zeros.

are taken to be of the same sign. Can we then reconstruct the bifurcation axis argument of the previous section along an s -axis which passes through the origin at an angle θ along which s increases linearly, with θ taking values between ϕ_2 and ϕ_3 (see Figure 11(a))? We search for points (s, θ) at which there is a second-order zero in the field parallel to the s -axis (B_\parallel), coincident with a first-order zero in the perpendicular field (B_\perp). If we can find such a second-order null, then we can conclude that, for the right perturbation to the source configuration, a local separator bifurcation will indeed occur.

3.3.1. Zeros in the Perpendicular Field

The main complication that arises with non-symmetric source configurations is that, due to the loss of symmetry, we no longer simply have a straight line along which the perpendicular field is zero. Since we are again considering an s -axis which runs through source 1, the perpendicular field (i.e., the field B_\perp perpendicular to the s -axis) depends only on sources 2 and 3. It is given by

$$B_\perp = \frac{F_3 A}{((s - G)^2 + A^2)^{3/2}} - \frac{F_2 B}{((s - H)^2 + B^2)^{3/2}}, \quad (5)$$

where

$$\begin{aligned} A &= r_3 \sin(\phi_3 - \theta), & B &= r_2 \sin(\theta - \phi_2), \\ G &= r_3 \cos(\phi_3 - \theta), & H &= r_2 \cos(\theta - \phi_2), \end{aligned}$$

and the negative θ direction is taken as the positive B_{\perp} direction. Hence $B_{\perp} = 0$ is given by

$$(1 - D)s^2 - 2(H - DG)s + (r_2^2 - Dr_3^2) = 0, \tag{6}$$

where

$$D = \left(\frac{F_2 r_2 \sin(\theta - \phi_2)}{F_3 r_3 \sin(\phi_3 - \theta)} \right)^{2/3}.$$

This is a quadratic in s , and hence, for a given value of θ , we may have two zeros, one zero, or no zeros, in the region of interest, $s > 0$, as shown in Figures 11(c–e), respectively. The number of zeros present depends on the sign of the determinant of (6), which is given by

$$4((H - DG)^2 - (1 - D)(r_2^2 - Dr_3^2)). \tag{7}$$

Consider now a fixed source configuration. What happens to the zeros in B_{\perp} as we vary θ from ϕ_2 to ϕ_3 (i.e., swing the bifurcation axis round from source 2 to source 3)? If the bifurcation axis passes close to source 2, then B_2 must dominate B_{\perp} for $s \approx r_2$, and similarly for source 3. What about the perpendicular field at infinity? Consider the parameterization in Figure 11(b). Then

$$\begin{aligned} B_{\perp} &= \frac{F_3 b}{(y^2 + b^2)^{3/2}} - \frac{F_2 a}{(x^2 + a^2)^{3/2}} \\ &\approx \frac{F_3 b - F_2 a}{s^3} \quad \text{as } s \rightarrow \infty. \end{aligned}$$

So the sign of B_{\perp} at infinity is given by the sign of $(F_3 b - F_2 a)$. Hence, if the bifurcation axis passes close to source 2, a is very small and source 3 dominates. Similarly, source 2 dominates at infinity if $\theta \approx \phi_3$. So for $\theta \approx \phi_2$ or ϕ_3 we have two zeros in B_{\perp} , close to r_2 or r_3 , respectively, as shown in Figure 12. As θ is varied from ϕ_2 to ϕ_3 , the field evolves between these two shapes, and may have one or no zeros for different values of θ .

We know the behavior of the zeros in B_{\perp} when $\theta \approx \phi_2$ or ϕ_3 , but what is the shape of the curve $B_{\perp} = 0$ in the whole $s - \theta$ plane? Some examples of the different possible topologies for this curve are shown in Figure 13.

Figure 13(a) shows the symmetric case from Section 3.2. Figure 13(b) is an example of the case where the determinant (7) is always positive, whereas in Figure 13(c) the determinant (7) is negative for intermediate values of θ , which implies there are no solutions to $B_{\perp} = 0$. The evolution between these topologies can be seen in Figure 14 where the single parameter F_3 is varied. The same effect can be achieved by varying the angle $(\phi_2 - \phi_3)$ or one of the lengths r_2 or r_3 .

3.3.2. Zeros in the Parallel Field

For a null point to be present in the magnetic field we require the zeros in the perpendicular field to coincide with zeros in the parallel field. We therefore now

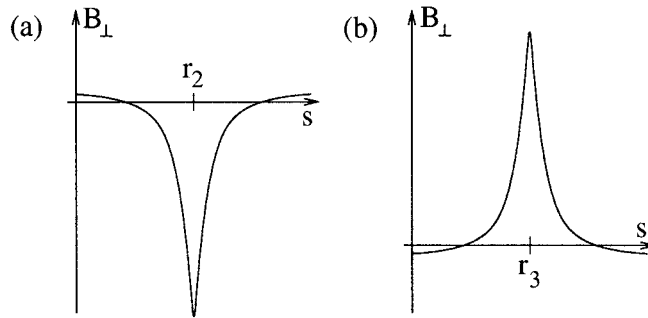


Figure 12. Schematic field profiles for B_{\perp} when (a) $\theta \gtrsim \phi_2$ and (b) $\theta \lesssim \phi_3$.

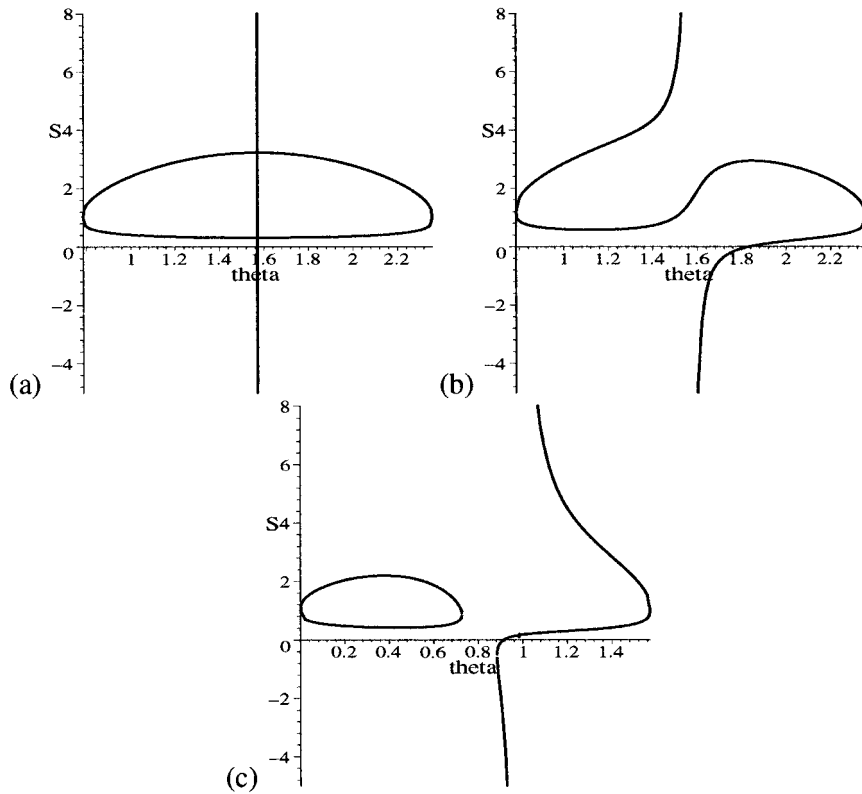


Figure 13. The curve $B_{\perp} = 0$ in the $s - \theta$ plane, for (a) the symmetric case; $r_2 = r_3 = 1$, $F_2 = F_3 = 1$, $\phi_2 = \pi/4$, $\phi_3 = 3\pi/4$, (b) $r_2 = 1.2$, $r_3 = 1$, $F_2 = 1$, $F_3 = 1.2$, $\phi_2 = \pi/4$, $\phi_3 = 3\pi/4$, and (c) $r_2 = 1.4$, $r_3 = 1$, $F_2 = 1$, $F_3 = 2$, $\phi_2 = \pi/4$, $\phi_3 = 3\pi/4$.

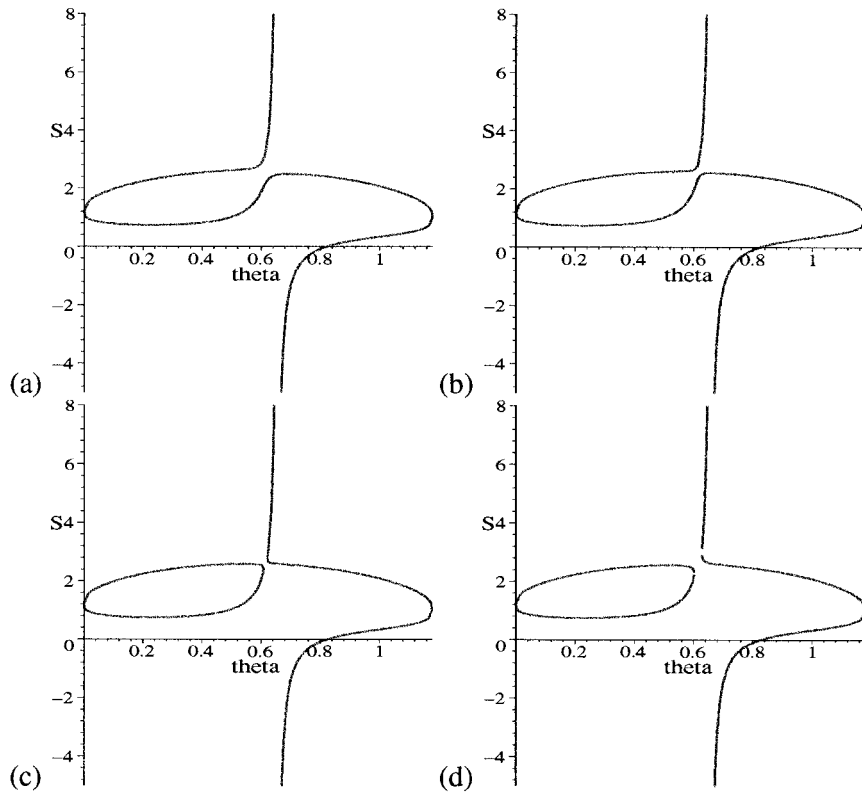


Figure 14. The curve $B_{\perp} = 0$ in the $s - \theta$ plane, for $r_2 = 1.2, r_3 = 1, F_2 = 1, \phi_2 = 0, \phi_3 = 3\pi/8$ and (a) $F_3 = 1.450$, (b) $F_3 = 1.460$, (c) $F_3 = 1.465$, and (d) $F_3 = 1.470$.

consider the field parallel to the bifurcation axis (B_{\parallel}), and try to apply the same argument as in the symmetric case.

The shape of the parallel field due to sources 2 and 3 ($B_{2+3\parallel}$) is observed to be the same as before (see Figure 15(a)). Hence, by the same argument as in the symmetric case, we can create a second-order zero in the parallel field by choosing F_1 so that the B_1 curve just touches the $-B_{2+3}$ curve. We find that the flux considerations are the same here as well; if source 1 is of opposite sign to sources 2 and 3 then we require $|F_1| > |F_2 + F_3|$ to obtain a second-order null. Figure 15(c) shows where $B_{\parallel} = 0$ in the $s - F_1$ plane, for a typical source configuration and typical value of θ . Note that when source 1 has opposite sign to sources 2 and 3 and $|F_1| < |F_2 + F_3|$, there is only one zero, and so there is a single first-order null in the parallel field.

We now want to plot the curve $B_{\parallel} = 0$ in the $s - \theta$ plane and look for its intersections with the $B_{\perp} = 0$ curve (Figure 13). Consider first extreme values of θ . For θ close to ϕ_2 , B_{\parallel} due to source 2 grows very large in magnitude as s approaches r_2 , at which point it drops to zero, and then becomes very large in the

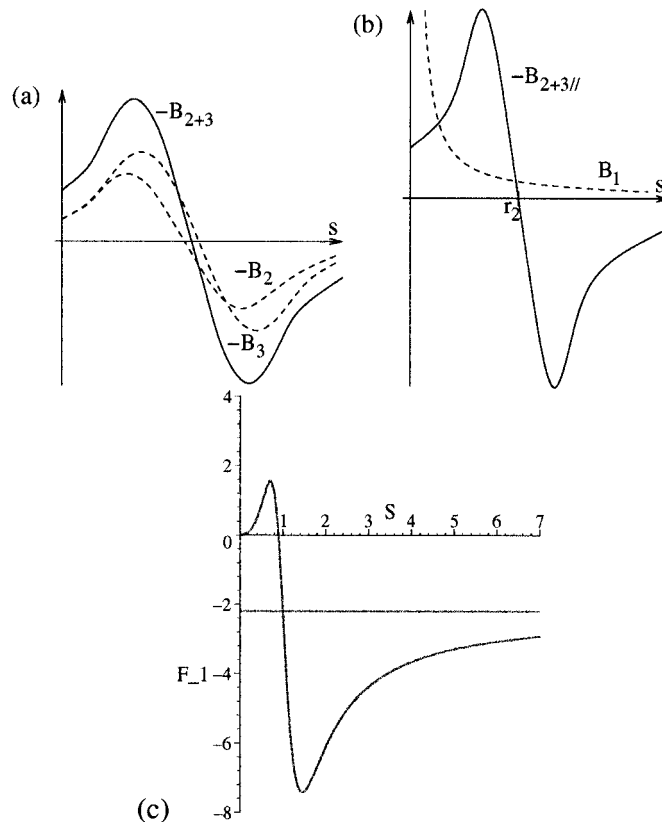


Figure 15. (a) Schematic diagram of $-B_{2+3||}$ for F_2 and F_3 positive. (b) Schematic of the parallel field when $\theta \approx \phi_2$. The dashed curve indicates a typical B_1 field profile for $F_1 > 0$ (for F_1, F_2, F_3 positive). (c) The position of nulls in the parallel field along $\theta = \pi/2$ as a function of F_1 for $r_2 = 1.1, r_3 = 1, F_2 = 1.2, F_3 = 1, \phi_2 = \pi/3$, and $\phi_3 = 2\pi/3$. The horizontal line indicates the value $-(F_2 + F_3)$ to which the curve tends asymptotically.

opposite direction when s is just greater than r_2 (see Figure 15(b)). We can see from Figure 15(b) that in this situation we have one zero of $B_{||}$ at $s \approx r_2$ and another at $s \ll r_2$. As θ increases, the $B_{2+3||} = 0$ curve flattens out, and the zeros move closer together. The same argument can be followed for $\theta \approx \phi_3$. Depending on the source strengths, and of course positions, the $B_{||} = 0$ curves in the $s - \theta$ plane should have one of the topologies shown schematically in Figure 16. Due to the shapes of these curves close to ϕ_2 and ϕ_3 , we can see that they must intersect the relevant $B_{\perp} = 0$ curve, to give the two standard first-order nulls we expect in a three-source configuration. But can there ever be a second-order null, and hence a bifurcation?

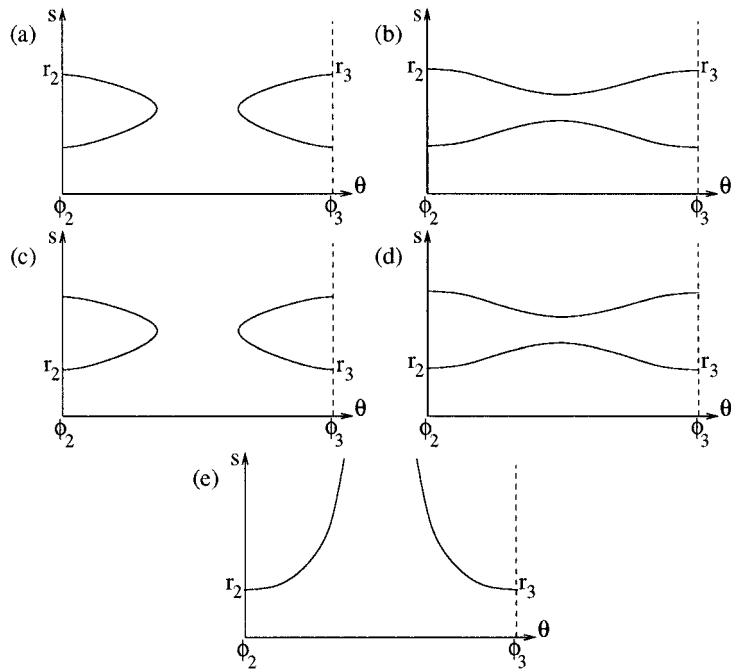


Figure 16. Schematic diagrams showing the curve $B_{\parallel} = 0$. When F_1 is the same sign as F_2 and F_3 , the curve may take shape (a) or (b). When F_1 is of opposite sign to F_2 and F_3 , it takes the shape (c), (d) or (e), where (c) and (d) correspond to $|F_1| > |F_2 + F_3|$ and (e) to $|F_1| < |F_2 + F_3|$.

3.3.3. Bifurcation to Touching State

In the following two subsections we search for examples of bifurcations, guided by the parameter values in Brown and Priest (1999) at which local separator bifurcations are observed to take place.

For bifurcation to the touching state we start in a separate or enclosed topological state with source 1 and sources 2 and 3 of opposite signs. Beginning with a source configuration which is close to symmetric and for which $B_{\perp} = 0$ gives one continuous curve as shown in Figure 13(b). We start with $F_1 = 1$, $F_2 = F_3 = -0.28$, $r_2 = 1$, $r_3 = 1.05$, $\phi_2 = 0$ and $\phi_3 = 0.45\pi$, and increase ϕ_3 . The resulting behavior of the curves $B_{\perp} = 0$ and $B_{\parallel} = 0$ is shown in Figure 17(a–c). Here it is the dashed section of the $B_{\perp} = 0$ curves which is cut an extra twice by the curve $B_{\parallel} = 0$. Plotting the value of the parallel field along this dashed curve for the different values of ϕ_3 , yields the three graphs shown in Figure 17(d).

We see clearly that when $\phi_3 = 0.45\pi$ and $\phi_3 = 0.7\pi$ there is one first-order zero in $B_{\parallel} = 0$, whereas when $\phi_3 = 0.57\pi$ there are three. So when $\phi_3 = 0.57\pi$ we have a total of four nulls and we must be in the touching state.

We can also have a local separator bifurcation when the $B_{\perp} = 0$ curve has the broken topology as in Figure 13(c). Figure 18 shows the bifurcation occurring as

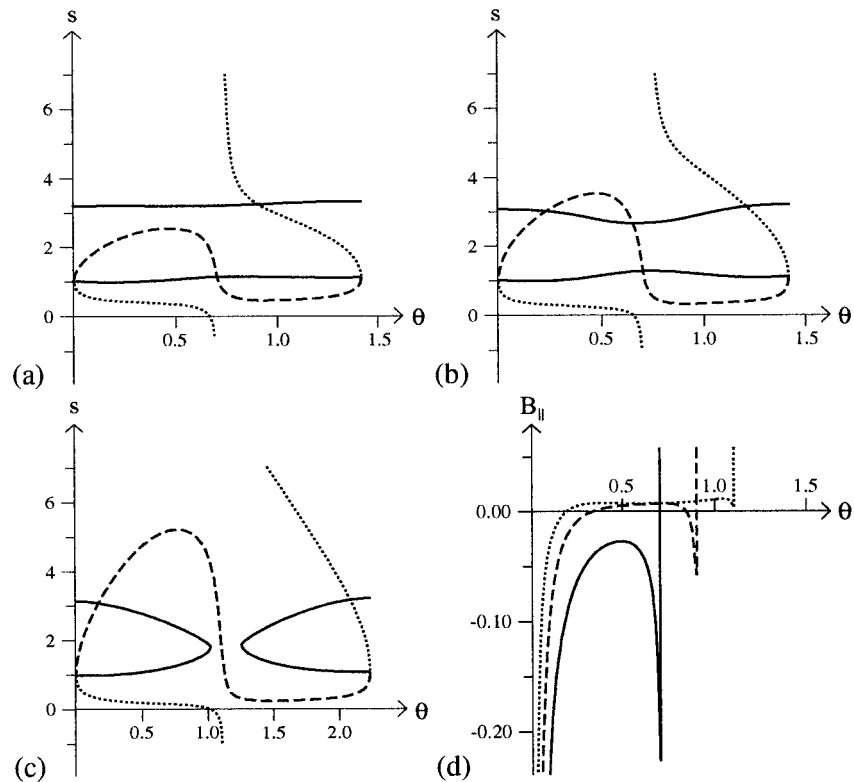


Figure 17. Zeros in the perpendicular and parallel fields for $\phi_3 =$ (a) 0.45π , (b) 0.58π , and (c) 0.71π . The *dashed curve* is the root of $B_{\perp} = 0$ reached by taking the '+' sign in the quadratic root formula (Equation (6)). The negative root is *dotted*, and the curve $B_{\parallel} = 0$ is the *solid line*. (d) B_{\parallel} plotted along the dashed part of $B_{\perp} = 0$ for $\phi_3 = 0.45\pi$ (*solid line*), 0.58π (*dashed*), and 0.71π (*dotted*). (a) corresponds to the separate state, (b) to the touching state, and (c) to enclosed state. Note that sources 2 and 3 are located where the solid line intersects the line $B_{\perp} = 0$ at the point where it changes from dotted to dashed.

before. This time, $F_1 = 1$, $F_2 = -0.28$, $F_3 = -0.33$, $r_2 = 1$, $r_3 = 1.05$, $\phi_2 = 0$ and again we vary ϕ_3 .

For highly non-symmetric source configurations, however, local separator bifurcations do not occur. For example, if we consider the same configuration as above, but this time with $F_3 = -0.75$, then, as ϕ_3 is varied from 0 to π , the shape of the B_{\parallel} curve along $B_{\perp} = 0$ is always similar to the solid curve shown in Figure 18(d).

3.3.4. Bifurcation to Triangular State

For bifurcation to the triangular state we start with a divided state with all of the sources the same sign, say positive. This time we start with configuration parameters as follows: $F_1 = 1$, $F_2 = F_3 = 1.5$, $r_2 = 1$, $r_3 = 1.05$, $\phi_2 = 0$ and $\phi_3 = 3\pi/8$. F_2 and F_3 are then decreased, and we see extra nulls appear. The intersections of

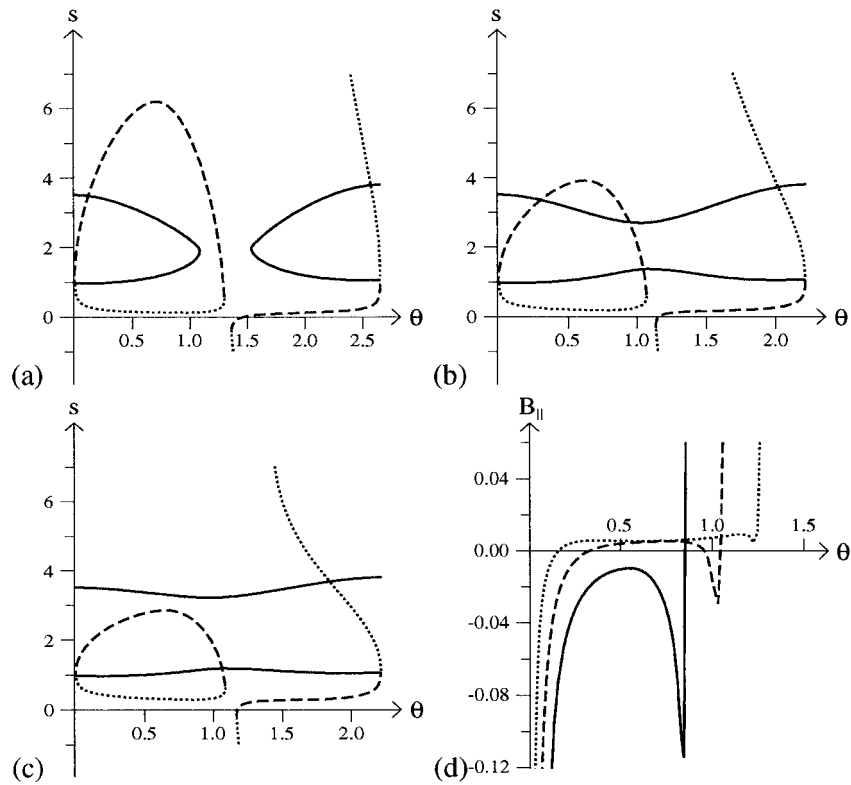


Figure 18. Zeros in the perpendicular and parallel fields for $\phi_3 =$ (a) 0.57π , (b) 0.7π , and (c) 0.84π . The dashed curve is the root of $B_{\perp} = 0$ reached by taking the ‘+’ sign in the quadratic root formula (Equation (6)). The negative root is dotted, and the curve $B_{\parallel} = 0$ is the solid line. (d) B_{\parallel} plotted along the dashed part of $B_{\perp} = 0$ for $\phi_3 = 0.57\pi$ (solid line), 0.7π (dashed), and 0.84π (dotted). (a) corresponds to the separate state, (b) to the touching state, and (c) to enclosed state.

the curves $B_{\perp} = 0$ and $B_{\parallel} = 0$ are shown in Figures 19(a–c) and the shape of B_{\parallel} along the dashed portion of $B_{\perp} = 0$ is shown in Figure 19(d).

Once again, this bifurcation can occur for more asymmetric cases than the ones described, though only up to a certain level of asymmetry.

In this section we have demonstrated that the results from Section 3, which discussed the symmetric case, are generic, and may be applied, with caution, to general non-symmetric configurations.

4. Conclusions

In this work we have put forward (for three sources) an explanation of the local separator bifurcation, which produces an important change of magnetic field topology. The analysis will hopefully allow us to predict the occurrence of such bifurcations for more complex fields due to higher numbers of sources, which commonly occur

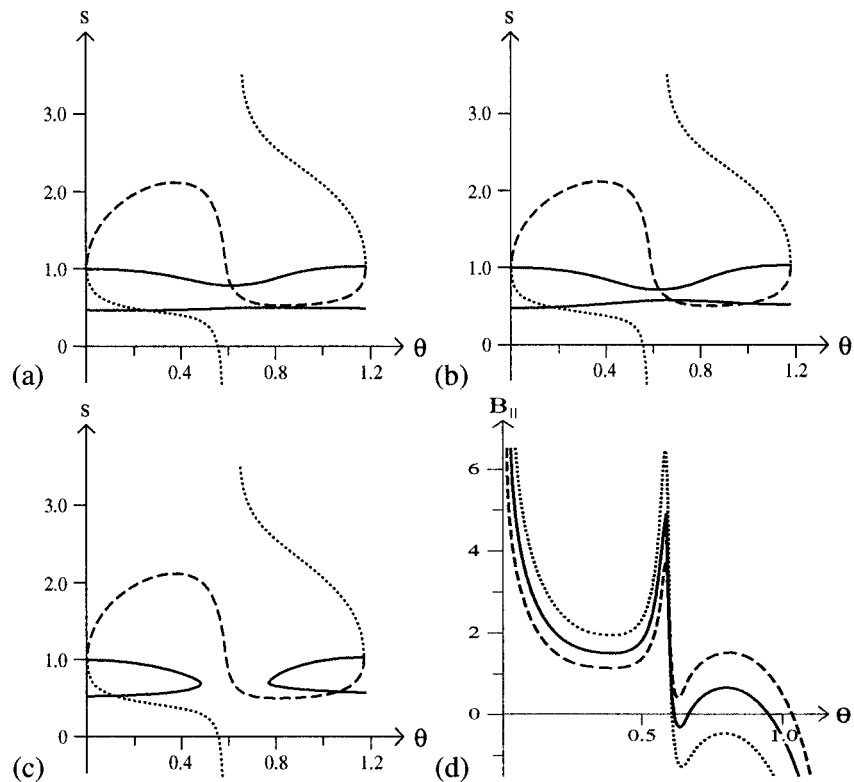


Figure 19. Zeros in the perpendicular and parallel fields for $F_2 = F_3 =$ (a) 1.5, (b) 1.1, and (c) 0.8. The *dashed curve* is the root of $B_{\perp} = 0$ reached by taking the '+' sign in the quadratic root formula (Equation (6)). The negative root is *dotted*, and the curve $B_{\parallel} = 0$ is the *solid line*. (d) B_{\parallel} plotted along the dashed part of $B_{\perp} = 0$ for $F_2 = F_3 = 1.5$ (*dotted curve*), 1.1 (*solid*), and 0.8 (*dashed*). (a) and (c) correspond to (globally) different divided states, and (b) to the triangular state.

in the solar corona, where the fields are often produced by an extremely complex network of flux fragments. This network evolves continually, and, as the topology of the resulting field changes, reconnective processes can trigger eruptive and heating events in the corona. However, the coronal field is thought to be largely made up of topological building blocks, resulting from small numbers of sources (Brown and Priest, 1999). So if we can explain topology and topology changes in these building blocks, we hope to develop an understanding of the structures of magnetic field which lead to dynamic events.

We have developed here a method of searching for local separator bifurcations by looking for second-order null points, which are the crucial field structure involved. In the three-source symmetric case we find that a bifurcation can always occur when all three sources have the same sign, as the source on the bifurcation axis is brought up. When the source-signs are not the same, the source of different sign must have a flux of greater magnitude than the sum of the fluxes of the other

two if we are to have a bifurcation. For non-symmetric source configurations the analysis is much more complicated and we cannot say too much in general about when bifurcations might occur, although for configurations ‘close’ to symmetric, we find the same as in the symmetric case. We plan to try and extend the analysis to symmetric cases for four or more sources to predict local separator bifurcations, and so use the present method to predict allowed topologies for more complex situations. In addition, when four or more sources are present, a *local double separator bifurcation* is also possible (Brown and Priest, 2001), which creates a new state with a null out of the photospheric plane in the corona. A method of predicting the birth of such coronal nulls would provide an invaluable tool for forecasting possible null reconnection sites.

Acknowledgements

D. I. Pontin would like to thank the Carnegie Trust, and E. R. Priest would like to thank the Particle Physics and Astronomy Research Council, for their financial support. This work has benefited greatly from helpful discussions with D. S. Brown. We are very grateful for the referee’s helpful comments.

References

- Berger, M. A.: 1986, *Geophys. Astrophys. Fluid Dynamics* **34**, 265.
 Brown, D. S. and Priest, E. R.: 1999, *Proc. R. Soc. London* **A455**, 3931.
 Brown, D. S. and Priest, E. R.: 2001, *Astron. Astrophys.* **367**, 339.
 Démoulin, P., Hénoux, J. C., and Mandrini, C. H.: 1992, *Solar Phys.* **139**, 105.
 Démoulin, P., Hénoux, J. C., and Mandrini, C. H.: 1994, *Astron. Astrophys.* **285**, 1023.
 Dubrovin, B. A., Fomenko, A. T., and Novikov, S. P.: 1990, *Modern Geometry – Methods and Applications*. Part II. *The Geometry and Topology of Manifolds*, Springer-Verlag, New York.
 Gorbachev, V. S.: 1988, ‘The Field Topology and Frozen-in Magnetohydrodynamic Flows of Plasma in the Strong-Field Approximation’. PhD thesis, Moscow Institute of Physics and Engineering.
 Hagenaar, H. J.: 2001, *Astrophys. J.* **555**, 448.
 Hornig, G. and Schindler, K.: 1996, *Phys. Plasmas* **3**, 781.
 Inverarity, G. W. and Priest, E. R.: 1999, *Solar Phys.* **186**, 99.
 Longcope, D. W.: 1996, *Solar Phys.* **169**, 91.
 Longcope, D. W.: 1998, *Astrophys. J.* **507**, 433.
 Parnell, C. E.: 2001, *Solar Phys.* **200**, 23.
 Priest, E. R. and Forbes, T. G.: 2000, *Magnetic Reconnection: MHD Theory and Applications*, Cambridge University Press, Cambridge.
 Priest, E. R. and Titov, V. S.: 1996, *Phil. Trans. R. Soc. London* **A354**, 2951.
 Priest, E. R., Bungey, T. N., and Titov, V.S.: 1997, *Geophys. Astrophys. Fluid Dynamics* **84**, 127.
 Schrijver, C. J. and Zwaan, C.: 2000, *Solar and Stellar Magnetic Activity*, Cambridge University Press, Cambridge.
 Schrijver, C. J., Title, A. M., Harvey, K. L., Sheeley, N. R., Wang, Y. -M., van den Oord, G. H. J., Shine, R. A., Tarbell, T. D., and Hurlburt, N. E.: 1998, *Nature* **394**, 152.
 Seehafer, N.: 1986, *Solar Phys.* **105**, 223.

Simon, G. W., Weiss, N. O., and Title, A. M.: 2001, *Astrophys. J.* **561**, 427.
Title, A. M.: 2000, *Phil. Trans. R. Soc. London* **A358**, 657.